Shelembe *et al.*
Journal of Analytical Science and Technology (2022) 13:8
https://doi.org/10.1186/s40543-022-00316-7

Journal of Analytical Science and Technology

RESEARCH ARTICLE Open Access

Biosynthesis and bioactivities of metal nanoparticles mediated by *Helichrysum aureonitens*

Bongisiwe Shelembe[1], Nomfundo Mahlangeni[1] and Roshila Moodley[1,2*]

Abstract

Biosynthesis of nanoparticles is the preferred route for the fabrication of biocompatible and cheaper drugs. In this study, the extract and major secondary metabolite from *Helichrysum aureonitens*, 3,5-dihydroxy-6,7,8-trimethoxyflavone, were used to synthesize silver and zinc oxide nanoparticles. Spectroscopic and microscopic techniques confirmed the formation of the nanoparticles. The flavone alone showed higher DPPH radical scavenging ability (IC_{50} = 487.1 µg mL^{-1}) relative to the control, butylated hydroxytoluene. In addition, silver nanoparticles synthesized using the flavone had higher ferric reducing potential (Fe^{3+} to Fe^{2+}) compared to the other test samples. The cytotoxic activity of the plant extract, the flavone, and their biosynthesized nanoparticles was also investigated using the MTT assay against the cancerous MCF-7 (breast adenocarcinoma) and A549 (human lung adenocarcinoma)), and non-cancerous HEK293 (human embryonic kidney) cell lines. The plant extract decreased the cell viability of A549 (IC_{50} = 68.6 µg mL^{-1}) without being cytotoxic against HEK293, even at high concentrations. Silver nanoparticles significantly decreased cell viability of A549 and moderately decreased cell viability of MCF-7 but induced cell death of HEK293 even at low concentrations. This study provides a green synthesis route for silver and zinc oxide nanoparticles and confirms the therapeutic effectiveness of *H. aureonitens*, thereby validating its use in ethnomedicine.

Keywords: Green synthesis, Flavonoids, Cytotoxicity, Antioxidant, Zinc oxide, Silver nanoparticles, *Helichrysum aureonitens*

Introduction

Cancer is among the leading causes of death worldwide (Miller et al. 2018). The uncontrollable cell growth that occurs can cause changes in biochemical and enzymatic parameters in the human body that results in the formation of tumors. Breast, lung, cervical, and esophageal cancer, among the deadliest cancers in South Africa, account for 19 160 deaths yearly (Nagai and Kim 2017). Globally, cancer is the second leading cause of death after cardiovascular diseases (Nagai and Kim 2017). According to the World Health Organization (WHO), 8.8 million cancer cases were reported in 2015; this figure is expected to increase up to 24 million by 2035 (Roy et al. 2018). Natural products play a significant role in human therapy, as they are a source of bioactive compounds that can provide leads for essential drugs that can either be synthesized as pharmaceuticals or extracted for traditional medicinal use. This drug leads to bridge the gap between conventional medicine and traditional medicine and account for approximately 60% of the therapeutic drugs in the market for cancer chemotherapy. Drug leads include flavonoids isolated from *Arabidopsis* that inhibit p-glycoprotein (mdir) in human cancer cells (Taylor and Grotewold 2005).

Helichrysum aureonitens Sch. Bip., known as everlasting (English) and impepho emhlophe (isiZulu), of the plant family Asteraceae and Compositae, is an indigenous

*Correspondence: moodleyrosh@ukzn.ac.za; roshila.moodley@manchester.ac.uk
[1] School of Chemistry and Physics, University of KwaZulu-Natal, Durban 4000, South Africa
Full list of author information is available at the end of the article

medicinal plant found in South Africa (Mathekga et al. 2000; Swartz 2006). The plant is used to prevent bed-wetting by children and treat wounds or infections and headaches (Leistner 1983; Meyer and Afolayan 1995). The chloroform and methanol extracts from *H. aureonitens* were reported to possess antibacterial activity, especially against *Micrococcus Kristinae* (MIC of 0.5 mg mL^{-1}), and the aqueous extract showed significant antiviral activity on herpes simplex virus type-1 (HSV-1) in human lung fibroblasts (1.35 mg mL^{-1}) (Meyer et al. 1997).

Nanoparticles are synthesized using various methods and by controlling various parameters. The use of plant extracts is reported to be environmentally friendly, relatively cheap, readily available, and easily scalable. Monodispersed nanoparticles with reduced size are reported to be more biocompatible than conventional therapeutics for drug encapsulation and drug delivery for the treatment of diseases such as cancer (Kim et al. 2007; Wang et al. 2008). Controlling experimental parameters such as pH can yield monodispersed nanoparticles (Singh et al. 2018). Nanoparticles of iron oxide, zinc oxide, and silver have previously been synthesized from plant material, and those tested for anticancer activity have demonstrated positive results (Premanathan et al. 2011; Sankar et al. 2013; Lakshmanan et al. 2018; Izadiyan et al. 2020). This study, therefore, aimed at synthesizing zinc oxide and silver nanoparticles using the extract and major isolated compound from *H. aureonitens*, which were then tested for their antioxidant and anticancer activities.

Materials and methods

General experimental procedures

Nuclear magnetic resonance (NMR) spectra were recorded by Bruker Advance III 400 and 600 MHz spectrometers (Germany) using deuterated methanol (CD_3OD) (Merck, Germany). Ultraviolet–visible (UV–Vis) spectra were recorded on a UV–Vis-NIR Shimadzu UV-3600 spectrophotometer over the wavelength range of 700–200 nm (Japan). Fourier-transform infrared spectroscopy (FTIR) spectra were recorded using a Perkin-Elmer Universal ATR spectrometer (USA). Gas chromatography–mass spectrometry (GC–MS) was performed on a Shimadzu GCMS-QP 2010SE instrument (Japan) equipped with a DB-5SIL MS (30 mm × 0.25 mm) fused silica capillary column (0.25 µm film thickness). Helium (2 mL min^{-1}) was used as a carrier gas. The column temperature was kept at 60 °C for 2 min then ramped to 300 °C for 30 min at a rate of 4 °C min^{-1}. The crystalline nature of nanoparticles was analyzed using powder X-ray diffraction (PXRD) and selected area electron diffraction (SAED) using a PANalytical X'Pert Pro, at a scanning rate of 2°/min and sample interval of 0.02° over the range $20° < 2\theta < 80°$. PXRD studies were conducted on a Bruker D8 Advance diffractometer with Cu Ka (l ¼ 1.5406 A) as the radiation source. The bioreduction of M^{n+} ions to M^0 was monitored by recording the maximum absorption peak obtained from UV–Vis spectroscopy (Shimadzu UV-1800 spectrophotometer, Japan) in a 200–800 nm wavelength range. The morphology and size of the nanoparticles were analyzed using transmission electron microscopy (TEM), JOEL JEM 1010, and JEOL JEM 2100 operated at a voltage of 100 and 200 kV, respectively. Scanning electron microscopy (SEM) images were taken using a FEG-SEM (Carl Zeiss, Germany) microscope operated at an accelerating voltage of 10 kV. EDX using the Oxford X max instrument was used to confirm that the elements present in the nanoparticles (Aztec Analysis Software, England).

Collection of plant material and preparation of extracts

The leaves from *H. aureonitens* were purchased from Warwick Durban Market, KwaZulu-Natal, South Africa, in June 2017 and identified by the taxonomist, Mr. Edward Khathi, School of Life Sciences. The voucher number, Shelembe B4, was deposited in the ward herbarium. Leaves were dried at room temperature for two weeks and crushed using a food blender (Salton, model SMS 15).

Extraction, isolation, and purification of compounds from *Helichrysum aureonitens*

Approximately 720 g of dried and crushed leaves were extracted for three days with 5 L of distilled methanol (MeOH) using an orbital shaker. The extract was concentrated using a rotary evaporator at a temperature that was 5 °C below the boiling point of the solvent, and then, the dried extract (2.83 g) was subjected to column chromatography with silica gel as a stationary phase (Merck Kieselgel 60, 0.063–0.200 mm, 70–230 mesh ASTM). Gradient elution using n-hexane and ethyl acetate (EtOAc) was employed for separation, starting with 100% hexane that was stepped by 10% to 100% EtOAc. Fractions (10 × 50 mL for each solvent system) were collected. TLC was used to evaluate the similarities and purity of each fraction. Fractions 21–35 were combined and further subjected to column chromatography to give compound 1.

Compound 1: ^{1}H-NMR ($CDCl_3$) δ_H 11.41 (1H, s, OH), 8.25 (2H, dd, J = 8.42 Hz and 1.06 Hz, H-2'/6'), 7.52 (3H, m, J = 7.52 Hz, H-3'/4'/5'), 6.69 (1H, s, OH), 4.10 (3H, s, OCH_3), 3.96 (3H, s, OCH_3), 3.94 (3H, s, OCH_3). ^{13}C-NMR ($CDCl_3$) δ_C 176.10 (C-4), 147.88 (C-), 145.25 (C-), 136.44 (C-), 130.83 (C-), 130.49 (C-), 130.02 (C-), 128.74 (C-), 127.72 (C-), 71.83 (C-), 62.09 (OCH_3), 61.72 (OCH_3), 61.18 (OCH_3).

Preparation of the aqueous extract and synthesis of nanoparticles

Finely ground leaves of *H. aureonitens* (20 g) were boiled in deionized water (200 mL) for 20 min then filtered by gravity. The filtrate was cooled to room temperature and stored at 4 °C for future use. Nanoparticles were only synthesized using the isolated compound and aqueous extract as these particles may be used in biomedical applications.

Silver nanoparticles (AgNPs)

An aqueous solution of silver nitrate (50 mL, 1 mM) was added dropwise (2 mL per minute) to the aqueous plant extract (50 mL). The solution was stirred overnight (8 h) at room temperature using a magnetic stirrer. A color change from orange to gray-black was observed. The suspended AgNPs were centrifuged at 5000 rpm for 30 min, washed several times with deionized water, and dried in an oven overnight at 50 °C. To synthesize AgNPs using compound 1, 10 mg of the compound was dissolved in 10 mL of MeOH and reacted with 10 mL of $AgNO_3$.

Zinc oxide nanoparticles (ZnONPs)

A solution of zinc chloride (50 mL, 0.4 M) was added to the aqueous plant extract (50 mL) dropwise. The solution was stirred at room temperature for 2 h. The pH of the solution was adjusted to 11 by adding a solution of NaOH (1.0 M) dropwise with constant stirring for 2 h at room temperature. The resulting precipitate was obtained after centrifugation at 5000 rpm for 30 min, washing several times with deionized water, and drying in an oven at 100 °C for 2 h.

Antioxidant activity (DPPH radical scavenging activity, ferric reducing antioxidant power, and phosphomolybdenum method)

According to the method described by Aliyu et al. (2013), the antioxidant potency of the crude extract, isolated compound, and their nanoparticles was evaluated using the stable free radical 2,2-diphenyl-1-picrylhydrazyl (DPPH) method. The standard antioxidants, ascorbic acid, α-tocopherol, and butylated hydroxytoluene (BHT), were used as positive controls. The absorbance was recorded at 517 nm using a UV–Vis spectrophotometer, and all experiments were conducted in triplicate.

The ferric reducing power of the test samples was determined according to the method described by Murthy et al. (2012). The absorbance was measured at 700 nm using a UV–Vis spectrophotometer with ascorbic, α-tocopherol, and BHT as positive controls and MeOH as a blank.

The total antioxidant capacity of the test samples using phosphomolybdenum was evaluated according to the method described by Aliyu et al. (2013). The absorbance was measured at 695 nm using a UV–Vis spectrophotometer with ascorbic acid, α-tocopherol, and BHT as positive controls and MeOH as a blank. For statistical purposes, all experiments were conducted in triplicate.

Cell viability and cytotoxicity testing

The cytotoxicity assay measures the ability of a compound to kill a targeted cell. The most common one used is the 3-[4,5-dimethylthiazol-2-yl]-2,5-diphenyltetrazolium bromide (MTT) assay. The crude extract, isolated compound, and nanoparticles synthesized from them were tested against three cell lines, namely, MCF-7 (breast adenocarcinoma), HEK 293 (human embryonic kidney), and A549 (human lung adenocarcinoma) originally obtained from the American Tissue Culture Collection (ATCC) (Virginia, USA). The cells were grown or seeded in a 25 mL tissue culture flasks in Eagle's minimum essential medium (EMEM) supplemented with 10% fetal bovine serum (FBS) and an antibiotic mixture of penicillin (100 μg mL^{-1}) and streptomycin (100 μg mL^{-1}). Cells at a plating cell density of 1.8×105 cells per well were plated into a 96 -well plate containing 200 μL medium. The cells were then incubated at 37 °C in 5% CO_2 and 95% air with 100% humidity overnight. After that, the medium was replaced with 200 μL of the freshly prepared medium.

Compounds to be tested were dissolved or suspended in 20% DMSO and diluted with phosphate buffer saline to make a total volume of 4 mL. Concentrations of 250, 125, 75, 30 μg mL^{-1} were added in triplicate to the cells in a 96-well plate and incubated for 48 h at 37 °C. A known anticancer agent (5-fluorouracil (5-FU)) was used as the positive control. MTT solution was added to each well and incubated for 3 h at 37 °C to form formazan salt, indicating cell viability (cell growth). The formazan salt was dissolved by adding DMSO (100 μL), forming a purple solution. The absorbance of the solution was read at 570 nm using a microplate reader. The absorbance is proportional to the number of viable cells in each well.

$$\%\text{Cell viability} = \frac{A_{\text{Sample}}}{A_{\text{untreated}}} \times 100$$

where A_{sample} is the absorbance of the sample and $A_{untreated}$ is the absorbance of the untreated cells. All experiments were carried out in triplicate.

Statistical analysis

The experimental data were expressed as mean ± standard deviation of three independent experiments. One-way analysis of variance (ANOVA) was performed on the data to evaluate significant differences between means using Tukey's post hoc test ($p < 0.05$). All statistical analyses were performed using GraphPad Prism 7.0 (GraphPad Software Inc., San Diego, CA).

Results and discussion

Structure elucidation of compound 1 from *Helichrysum aureonitens*

Compound 1 was isolated as a yellow amorphous solid with a mass of 15 mg. GC–MS data showed a molecular ion peak at *m/z* [M^+] 344.09, which corresponds to the molecular formula, $C_{18}H_{16}O_7$. The ^{1}H NMR spectrum showed characteristic resonances for flavonoids at δ_H 8.25 (H-2'/6'), 7.52–7.48 (H-3'/4'/5') from the B ring. No signal around δ_H 5 indicated that ring A (resorcinol moiety) is fully substituted. The three resonances at δ_H 4.10, 3.96, 3.94, integrating to 3 protons each indicated three methoxy groups that correlated with carbon resonances at δ_C 61.18, 61.72, and 62.09, respectively, from the HSQC experiment. The spectral data matched those previously reported and mass data confirmed compound 1 to be 3,5-dihydroxy-6,7,8-trimethoxyflavone (Additional file 1) (Wollenweber et al. 1993; Süzgeç et al. 2005; Xiong et al. 2009). Based on our knowledge, this compound is reported for the first time in the species. The flavone was the major compound in the extract of *H. aureonitens* and was used to synthesize nanoparticles and the aqueous extract.

Characterization of biosynthesized nanoparticles

Plants contain phytocompounds with the potential to reduce and stabilize metals to form nanoparticles. In this study, the flavone isolated from the *H. aureonitens* extract acted as a reducing and capping agent. The mechanism of metal coordination to flavones usually occurs via hydroxyl and carbonyl groups of the C ring; the coordination is called 3–4 site or 4–5 site or both (Fig. 1) (Kulkarni and Muddapur 2014).

The formation of nanoparticles was depicted by a color change of the *H. aureonitens* extract and the flavone to a gray-black indicating reduction of Ag^+ to Ag^0 for AgNPs and the formation of white suspension indicating the reduction of Zn^{2+} to Zn^0 for ZnONPs.

The UV–Vis spectra of the AgNPs and ZnONPs synthesized using both the *H. aureonitens* extract and flavone showed a distinct peak around 429 nm and 280 nm due to surface plasmon resonance (Fig. 2). The absorption peak for AgNPs from the extract appeared sharper than that from the flavone, with peak broadness indicating polydispersity of nanoparticles. These results were consistent with previous studies that showed absorption peaks between 410 and 430 nm for AgNPs (Lakshmanan et al. 2018) and 362 nm for ZnONPs (Premanathan et al. 2011). A red shift was observed for ZnONPs indicative of larger particles with different shapes from that obtained by Premanathan and co-worker (Premanathan et al. 2011).

The TEM images of AgNPs synthesized from the extract of *H. aureonitens*, and the flavone are shown in Fig. 3. The TEM image (Fig. 3a, d) indicated spherical particles with agglomeration. The SEM image (Additional

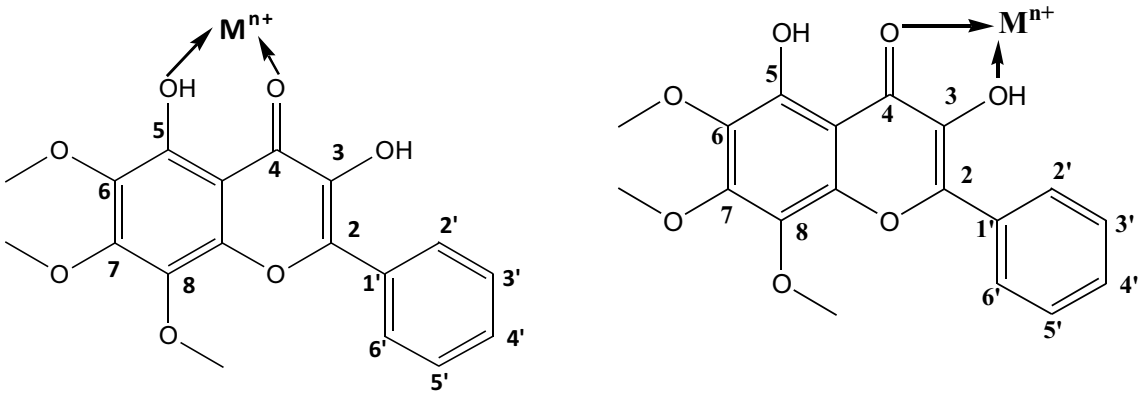

Fig. 1 Possible chelating coordination sites ((3–4) and (4–5)) for the isolated flavone (3,5-dihydroxy-6,7,8-trimethoxyflavone). M^{n+} denotes metal ions, which can be either Ag^+ or Zn^{2+}

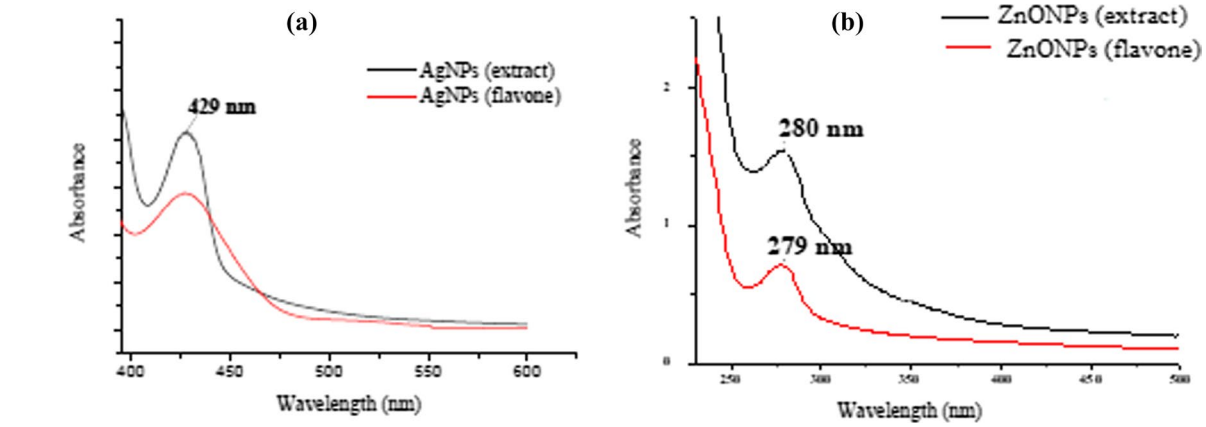

Fig. 2 UV spectra of **a** AgNPs and **b** ZnONPs synthesized using *H. aureonitens* extract and isolated flavone

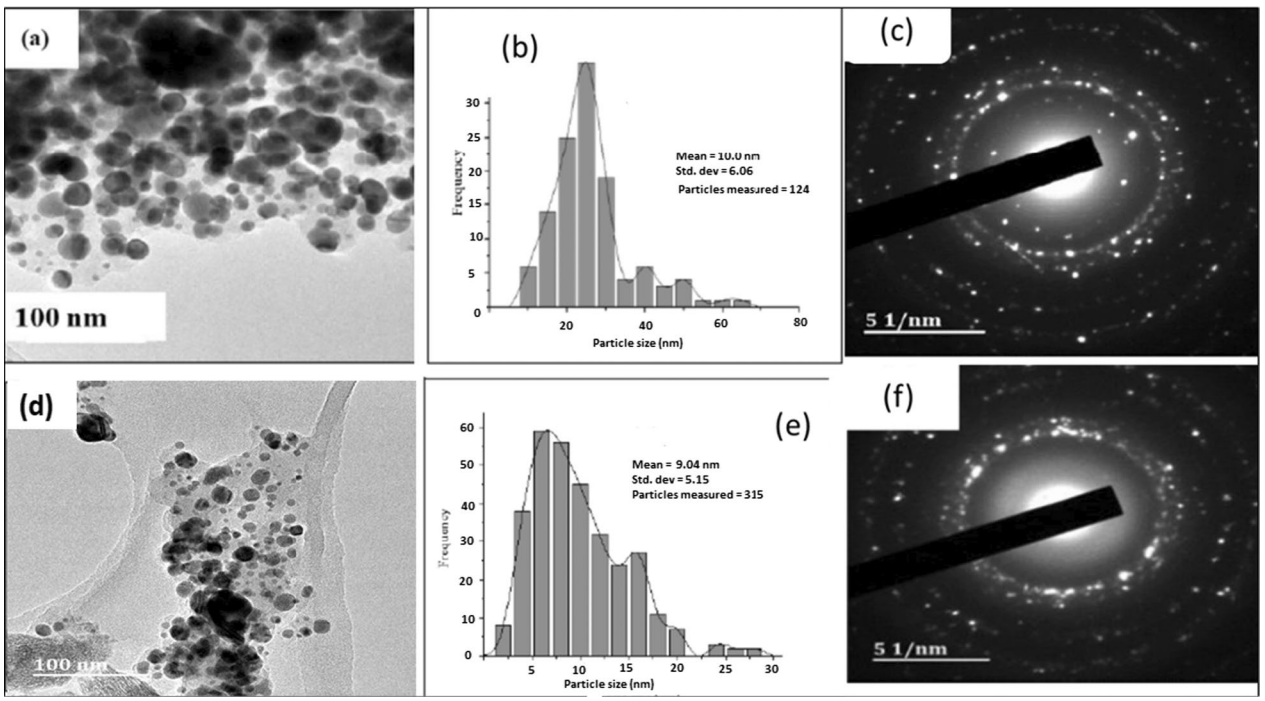

Fig. 3 TEM Images, particle size distribution histogram and SAED pattern of AgNPs synthesized using *H. aureonitens* extract (**a**–**c**) and flavone (**d**–**f**)

file 1) confirmed particles to be spherical. The particle size distribution histogram, as measured by TEM images (Fig. 3b, e), showed particle sizes to range between 5 and 65 nm (from the extract) with an average size of 10 nm, which supports the UV–Vis data. The nanoparticles synthesized using the flavone showed particle sizes that ranged between 3 and 29 nm with an average size of 9.0 nm. The SAED pattern showed concentric diffraction rings as bright spots indicating that both are crystalline particles (Fig. 3c, f). The d-spacing was also measured from the lattice fringes and the lattice spacings obtained were 0.234, 0.201, 0.139, 0.124 and 0.119 nm that matched exactly to the (111), (200), (220), (222) and (311). This was compared to literature and indexed to the facet of a face-centered cubic crystal structure of AgNPs (Ahmad et al. 2010; Kora et al. 2012).

The microscopic characterization of ZnONPs synthesized from the extract and flavone is presented in Fig. 4. Nanoparticles synthesized from the extract appeared to be spheres or spheres joined together to form rods or

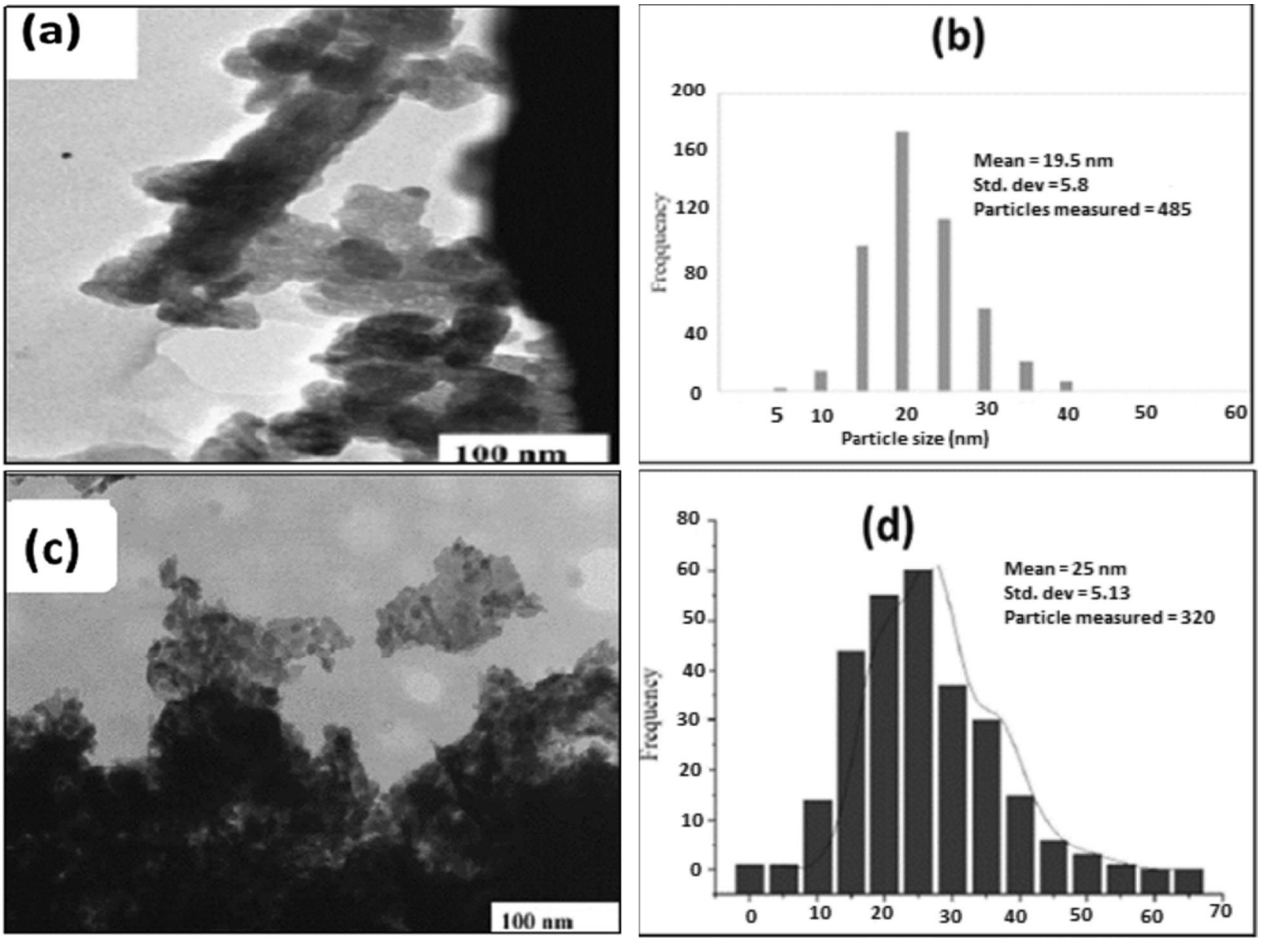

Fig. 4 TEM Images and particle size distribution histogram of ZnONPs synthesized using *H. aureonitens* extract (**a**, **b**) and flavone (**c**, **d**)

needles. The TEM image confirmed this where it showed agglomerated spheres surrounding the thread-like or rod particles (Fig. 4a), with particle size distribution histograms showing particle sizes that ranged between 7 and 45 nm with an average size of 19 nm (Fig. 4b). Nanoparticles synthesized using the flavone showed agglomerated spherical nanoparticles (Fig. 4c). The nanoparticle sizes ranged between 0.5 and 68 nm, with an average size of 25 nm (Fig. 4d).

The EDX spectra from the crude extract and flavone are shown in Fig. 5a and c, respectively; Zn and O are presented as significant elements with traces of C due to carbon-containing phytocompounds and Cl that originated from traces of the starting material, zinc chloride. The diffraction peaks observed at 2θ of 31.76°, 34.42°, 36.25°, 47.50°, 56.60°, 62.86°, 67.96° and 69.33° corresponding to the lattice planes (100), (002), (101), (102), (110), (103), (112), and (201) of PXRD in Fig. 5b and d. According to the PXRD pattern, both the synthesized ZnONPs showed a classic hexagonal crystal Wurtzite structure. The characteristic peaks at 2θ of 31.8°, 34.4°, 36.3°, 47.5°, 56.6°, 62.9° and 67.9° were assigned to the (100), (002), (101), (102), (110), (103) and (112) lattice planes, which corresponds to the wurtzite structure of ZnONPs. The most substantial diffraction peak was observed at $2\theta = 36°$, corresponding to ZnO's (101) lattice planes. This phase was similar for both nanoparticles.

Antioxidant activity

For this study, the commonly used assays (DPPH, FRAP, and phosphomolybdenum) were employed to evaluate the antioxidant activity of the aqueous extract of *H. aureonitens*, flavone (3,5-dihydroxy-6,7,8-trimethoxyflavone), and nanoparticles (ZnONPs and AgNPs) synthesized from both the aqueous extract and flavone.

The DPPH radical scavenging ability of the crude extract, flavone, and their nanoparticles are shown in Fig. 6. Ascorbic acid, BHT, and tocopherol are known for their antioxidant activity and are therefore used as positive controls. Ascorbic acid and tocopherol showed

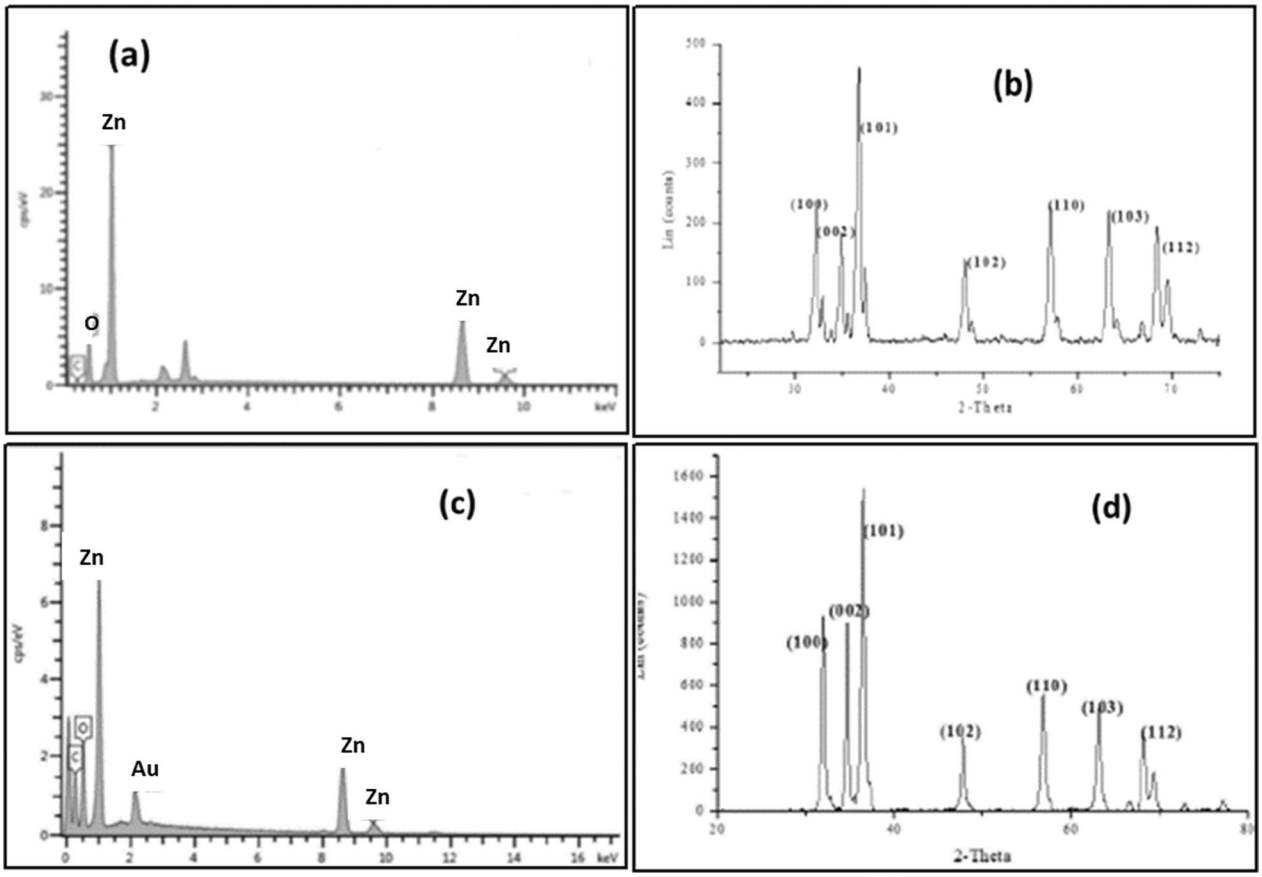

Fig. 5 EDX spectra and PXRD diffraction patterns of ZnONPs synthesized using *H. aureonitens* extract (**a**, **b**) and flavone (**c**, **d**)

high activity as expected with IC_{50} values of 78.22 and 223.4 μg mL^{-1}, respectively. The flavone showed higher antioxidant activity than BHT, with an IC_{50} of 487.1 μg mL^{-1}. The crude extract also exhibited better scavenging activity but lower than that of the flavone. Previous studies have shown flavonoids to possess good radical scavenging activity, attributed to the phenolic hydroxide groups attached to their structures (Van Acker et al. 1996; Amić et al. 2003). The hydroxyl group at position 3 of the C-ring and position 5 of the A-ring, which can be donated, enhances the radical scavenging activity of the isolated flavone. The double bond at C2–C3 conjugated with a 4-keto group facilitates electron delocalization, stabilizing the radical flavone formed (Amić et al. 2003). The activity is also improved by combining a double bond at C2-C3 with the 3-OH; this was observed by the improved scavenging ability of quercetin compared to other catechol flavonoids (Van Acker et al. 1996).

The scavenging ability of the nanoparticles was lower than their reducing and stabilizing agents. However, AgNPs showed better antioxidant activity than ZnONPs, with the scavenging potential of AgNPs (flavone) being significantly higher than AgNPs (*H. aureonitens* extract). Smaller nanoparticles (AgNPs (flavone)) have a large surface area and hence better interaction with biological systems and more flavone is attached to the surface of the nanoparticles. Our results agree with previous studies that correlate particle size and shape to biological activities (Sahu et al. 2016).

The electron-donating ability of the *H. aureonitens* extract, flavone, and the synthesized nanoparticles was measured by the FRAP assay to reduce Fe^{3+} to Fe^{2+} ions. AgNPs synthesized by the flavone had higher activity than the other test samples, including that of the flavone. The phosphomolybdenum method is based on the reduction of molybdenum (VI) by the antioxidants to the molybdenum (V) complex, which absorbs at 695 nm (Srinivasahan and Durairaj 2014). The flavone had higher reducing power on molybdenum (VI) ions than ascorbic acid, and tocopherol and AgNPs synthesized from the flavone exhibited higher antioxidant activity than the other nanoparticles.

The three assays confirmed that the antioxidant activity of the flavone, whether by radical scavenging or reducing

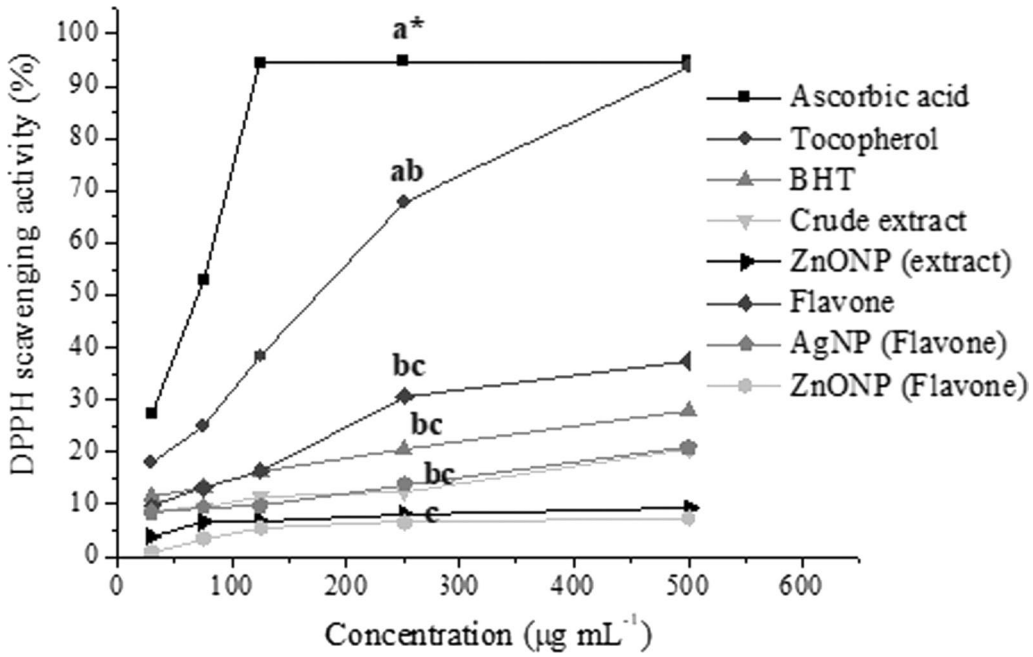

Fig. 6 DPPH radical scavenging activity of *H. aureonitens* extract, flavone and nanoparticles (AgNPs and ZnONPs) synthesized using *H. aureonitens* extract and isolated flavone. Ascorbic acid, tocopherol and butylated hydroxytoluene (BHT) were used as controls. Different alphabets indicate mean separation by Turkey's post hoc test ($p < 0.05$)

ability, is better than that of the extract. Therefore, the combined antioxidant activity of the compounds present in the plant is antagonistic. The assays also confirmed that the radical scavenging and reducing abilities of AgNPs are better than ZnONPs. The synergy between the flavone and AgNPs ameliorated the activity of the flavone-synthesized AgNPs.

In vitro cytotoxicity assay

The cytotoxic effect of the extract *of H. aureonitens*, flavone, and their nanoparticles (ZnONPs and AgNPs) was investigated on three cell lines, the cancerous A549 (human lung carcinoma) and MCF-7 (human breast carcinoma), and non-cancerous HEK293 (human embryonic kidney) cell lines. The cells were treated with different concentrations of test samples and evaluated using the MTT cell viability assay. A color change from yellow to purple indicated the formation of formazan crystals dependent on NADPH and oxidoreductase enzymes in the cytosolic compartment of the cell. Therefore, the purple color is directly proportional to cell viability (cell growth).

An expected trend of decreasing cell viability with increasing concentration of test samples was observed in the cancerous and non-cancerous cell lines (Fig. 7). The IC_{50} values of the *H. aureonitens* extract, flavone, and nanoparticles were compared to the known anticancer drug, 5-fluorouracil (5-FU) as shown in Table 1. Untreated cells (UN) were used as a negative control for each cell line. The IC_{50} values were estimated using nonlinear regression. The extract from *H. aureonitens* showed extreme selectivity towards A549 with an IC_{50} value of 68.6 μg mL^{-1} without being cytotoxic against the non-cancerous HEK293, even at high concentrations.

AgNPs from *H. aureonitens* extract, and the flavone significantly decreased cell viability of A549 and moderately decreased cell viability of MCF-7, respectively, and ZnONPs (flavone) significantly reduced cell viability of MCF-7. Their activity was not significantly different from the positive control, 5FU, which agreed with the finding obtained by Reshma and Mohanan (2017) for these metal nanoparticles. AgNPs (from both the extract and flavone) were more cytotoxic against A549 than the positive control. However, it was found to induce cell death of non-cancerous cells HEK293 even at low concentrations.

ZnONPs (flavone) were more selective toward A549 than MCF-7 but were also cytotoxic toward HEK293. Capping metals with the phytocompounds improved the activity of the compounds against the cell lines tested, which was observed by a decrease in cell viability. All nanoparticles decreased cell viability in all three cell lines in a dose-dependent manner. They also showed selectivity toward A549 compared to MCF-7. For both of the

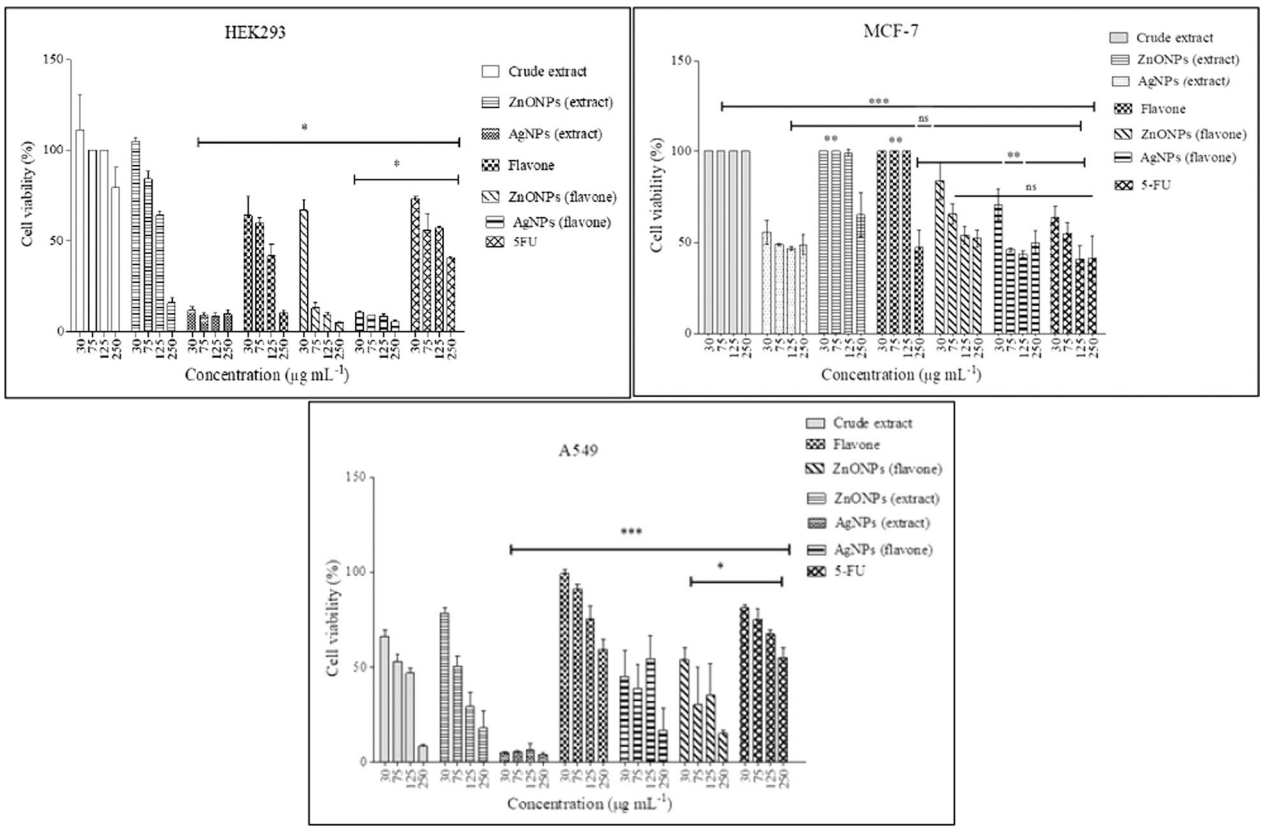

Fig. 7 MTT cell viability results for non-cancerous HEK293 and cancerous A549 and MCF-7 cell lines after treating with *H. aureonitens* extract, flavone, their nanoparticles (ZnONPs and AgNPs), and 5-fluorouracil, 5-FU. Significant differences (*$p < 0.05$, **$p < 0.005$, ***$p < 0.001$) are relative to 5-FU

Table 1 IC_{50} values of the crude extract, flavone and nanoparticles synthesized from *H. aureonitens* on HEK293, A549, and MCF-7 cell lines and DPPH

Compounds	IC_{50} values in µg mL^{-1}			
	HEK293	A549	MCF-7	DPPH
Crude extract	250.0	68.6	> 250	> 600
AgNP (*H. aureonitens*)	< 30	250.0	69.04	> 600
ZnONP (*H. aureonitens*)	> 250	76.89	232.3	> 600
Flavone	142.4	116.6	> 250	487.1
AgNP (Flavone)	58.24	250.0	30.29	> 600
ZnONP (Flavone)	< 30	< 30	70.16	> 600
5-Fluorouracil	46.42	74.31	> 250	
Ascorbic acid	–	–	–	78.22
Tocopherol	–	–	–	223.4
Butylated hydroxytoluene	–	–	–	> 600

cancerous cell lines tested, AgNPs and ZnONPs' activity was comparable when capped with the flavone; however, AgNPs showed better activity than ZnONPs when capped with compounds from the extract. AgNPs synthesized by flavonoids are generally more cytotoxic, and toxicity is based on nanoparticles' different surface properties and interaction time (Sahu et al. 2016).

Conclusions

The major secondary metabolite isolated from *H. aureonitens* was identified as the flavone (3,5-dihydroxy-6,7,8-trimethoxyflavone). AgNPs and ZnONPs were successfully synthesized using the flavone and the aqueous extract, and both types of particles exhibited size ranges of 2–35 nm. All of the test samples demonstrated antioxidant ability by scavenging free radicals or reducing metal ions by donating an electron. Nanoparticles synthesized using the flavone and aqueous extract showed moderate to low antioxidant activity and high cytotoxic activity against cancerous and non-cancerous cell lines. The aqueous extract showed selective cytotoxic activity towards A549 (human lung carcinoma), highlighting the potential of the crude extract from *H. aureonitens* to treat lung cancer. This study reveals the therapeutic effectiveness and metal-reducing ability of the compounds

present in *H. aureonitens*, thereby validating its ethnomedicinal use and confirming its ability to synthesize nanoparticles using a green approach, respectively.

Abbreviations

AgNPs: Silver nanoparticles; DPPH: 2,2-Diphenyl-1-picrylhydrazyl; EDX: Energy-dispersive X-ray spectroscopy; FTIR: Fourier-transform infrared spectroscopy; MTT: 3-[4,5-Dimethylthiazol-2-yl]-2,5-diphenyltetrazolium bromide; NMR: Nuclear magnetic resonance spectroscopy; PXRD: Powder X-ray diffraction; SAED: Selected area electron diffraction; SEM: Scanning electron microscopy; TEM: Transmission electron microscopy; ZnONPs: Zin oxide nanoparticles.

Supplementary Information

The online version contains supplementary material available at https://doi.org/10.1186/s40543-022-00316-7.

Additional file 1: Supplementary Information**.**

Acknowledgements

The authors would like to thank the National Research Foundation (NRF) and UKZN Nanotechnology Platform for funding and the University of KwaZulu-Natal (UKZN) for their facilities. We would also like to acknowledge Dr. Judie Magura in the Physiology Department (UKZN), and Dr. Vuyisa Mzozoyana in the Chemistry Department (UKZN).

Authors' contributions

BS involved in conceptualization, investigation, data interpretation, writing—original draft, and writing—review and editing. NM involved in data interpretation and writing—review and editing. RM involved in project supervisor, conceptualization, and writing—review and editing. All authors read and approved the final manuscript.

Funding

This work was supported by the National Research Foundation (Grant Nos. 114008, 95100, 111234).

Availability of data and materials

All data generated or analyzed during this study are included in this published article and its Additional file 1.

Declarations

Competing interests

The author(s) declare(s) that there is no conflict of interest regarding the publication of this article.

Author details

[1]School of Chemistry and Physics, University of KwaZulu-Natal, Durban 4000, South Africa. [2]Department of Chemistry, University of Manchester, Oxford Rd, Manchester M13 9PL, UK.

Received: 13 August 2021 Accepted: 23 February 2022
Published online: 18 March 2022

References

Ahmad N, Sharma S, Alam MK, et al. Rapid synthesis of silver nanoparticles using dried medicinal plant of basil. Colloids Surf B Biointerfaces. 2010;81:81–6. https://doi.org/10.1016/j.colsurfb.2010.06.029.

Aliyu AB, Ibrahim MA, Musa AM, et al. Free radical scavenging and total antioxidant capacity of root extracts of *Anchomanes difformis* ENGL. (ARACEAE). Acta Pol Pharm Drug Res. 2013;70:115–21.

Amić D, Davidović-Amić D, Bešlo D, Trinajstić N. Structure-radical scavenging activity relationships of flavonoids. Croat Chem Acta. 2003;76:55–61.

Izadiyan Z, Shameli K, Miyake M, et al. Cytotoxicity assay of plant-mediated synthesized iron oxide nanoparticles using *Juglans regia* green husk extract. Arab J Chem. 2020;13:2011–23. https://doi.org/10.1016/j.arabjc.2018.02.019.

Kim JS, Kuk E, Yu KN, et al. Antimicrobial effects of silver nanoparticles. Nanomed Nanotechnol Biol Med. 2007;3:95–101. https://doi.org/10.1016/j.nano.2006.12.001.

Kora A, Beedu S, Jayaraman A. Size-controlled green synthesis of silver nanoparticles mediated by gum ghatti (*Anogeissus latifolia*) and its biological activity. Org Med Chem Lett. 2012;2:17. https://doi.org/10.1186/2191-2858-2-17.

Kulkarni N, Muddapur U. Biosynthesis of metal nanoparticles: a review. J Nanotechnol. 2014. https://doi.org/10.1155/2014/510246.

Lakshmanan G, Sathiyaseelan A, Kalaichelvan PT, Murugesan K. Plant-mediated synthesis of silver nanoparticles using fruit extract of *Cleome viscos*a L.: assessment of their antibacterial and anticancer activity. Karbala Int J Mod Sci. 2018;4:61–8. https://doi.org/10.1016/j.kijoms.2017.10.007.

Leistner OH (1983) Flora of Southern Africa (Asteraceae) Botanical Research Institute of South Africa

Mathekga ADM, Meyer JJM, Horn MM, Drewes SE. An acylated phloroglucinol with antimicrobial properties from *Helichrysum caespititium*. Phytochemistry. 2000;53:93–6. https://doi.org/10.1016/S0031-9422(99)00424-0.

Meyer JJM, Afolayan AJ. Antibacterial activity of *Helichrysum Aureonitens* (Asteraceae). J Ethnopharmacol. 1995;47:109–11.

Meyer JJM, Afolayan AJ, Taylor MB, Erasmus D. Antiviral activity of galangin isolated from the aerial parts of *Helichrysum aureonitens*. J Ethnopharmacol. 1997;56:165–9. https://doi.org/10.1016/S0378-8741(97)01514-6.

Miller KD, Siegel RL, Khan R, Jemal A. Cancer statistics. Cancer Rehabil Princ Pract. 2018. https://doi.org/10.3322/canjclin.40.5.318.

Murthy PS, Manjunatha M, Sulochannama G, Madhava Naidu M. Extraction, characterization and bioactivity of coffee anthocyanins. Eur J Biol Sci. 2012;4:13–9.

Nagai H, Kim YH. Cancer prevention from the perspective of global cancer burden patterns. J Thorac Dis. 2017;9:448–51. https://doi.org/10.21037/jtd.2017.02.75.

Premanathan M, Karthikeyan K, Jeyasubramanian K, Manivannan G. Selective toxicity of ZnO nanoparticles toward Gram-positive bacteria and cancer cells by apoptosis through lipid peroxidation. Nanomed Nanotechnol Biol Med. 2011;7:184–92. https://doi.org/10.1016/j.nano.2010.10.001.

Reshma VG, Mohanan PV. Cellular interactions of zinc oxide nanoparticles with human embryonic kidney (HEK 293) cells. Colloids Surf B Biointerfaces. 2017;157:182–90. https://doi.org/10.1016/j.colsurfb.2017.05.069.

Roy A, Jauhari N, Bharadvaja N. Medicinal plants as a potential source of chemopreventive agents BT. In: Akhtar MS, Swamy MK, editors. Anticancer plants: natural products and biotechnological implements, vol. 2. Singapore: Springer Singapore; 2018. p. 109–39.

Sahu N, Soni D, Chandrashekhar B, et al. Synthesis of silver nanoparticles using flavonoids: hesperidin, naringin and diosmin, and their antibacterial effects and cytotoxicity. Int Nano Lett. 2016;6:173–81. https://doi.org/10.1007/s40089-016-0184-9.

Sankar R, Karthik A, Prabu A, et al. *Origanum vulgare* mediated biosynthesis of silver nanoparticles for its antibacterial and anticancer activity. Colloids Surf B Biointerfaces. 2013;108:80–4. https://doi.org/10.1016/j.colsurfb.2013.02.033.

Singh A, Singh NB, Afzal S, et al. Zinc oxide nanoparticles: a review of their biological synthesis, antimicrobial activity, uptake, translocation and biotransformation in plants. J Mater Sci. 2018;53:185–201. https://doi.org/10.1007/s10853-017-1544-1.

Srinivasahan V, Durairaj B. Antioxidant and free radical scavenging effect of *Morinda citrifolia* fruit extract. Int J Pharm Pharm Sci. 2014;6:55–9.

Süzgeç S, Meriçli AH, Houghton PJ, Çubukçu B. Flavonoids of *Helichrysum compactum* and their antioxidant and antibacterial activity. Fitoterapia. 2005;76:269–72. https://doi.org/10.1016/j.fitote.2004.12.006.

Swartz VG (2006) Phytochemical studies of *Helichrysum patulum*. M.Sc. University of the Western Cape.

Taylor LP, Grotewold E. Flavonoids as developmental regulators. Curr Opin Plant Biol. 2005;8:317–23. https://doi.org/10.1016/j.pbi.2005.03.005.

Van Acker SABE, Van Den Berg DJ, Tromp MNJL, et al. Structural aspects of antioxidant activity of flavonoids. Free Radic Biol Med. 1996;20:331–42. https://doi.org/10.1016/0891-5849(95)02047-0.
Wang X, Yang L, Chen Z, Shin DM. Application of nanotechnology in cancer therapy and imaging. CA Cancer J Clin. 2008;58:97–110. https://doi.org/10.3322/ca.2007.0003.
Wollenweber E, Fritz H, Henrich B, et al. Rare flavonoid aglycones from *Anaphalis margaritacea* and two *Gnaphalium* species. Zeitschrift Fur Naturforsch Sect C J Biosci. 1993;48:420–4. https://doi.org/10.1515/znc-1993-5-604.
Xiong HP, Wu ZJ, Chen FT, Chen WS. 5,7-Dihydroxy-3,6,8-trimethoxyflavone. Acta Crystallogr Sect E Struct Rep. 2009;E65:o3276–7. https://doi.org/10.1107/S1600536809050715.

Publisher's Note